COLLAPSE FRAGILITY CURVES FOR SEISMIC ASSESSMENT OF SUPERPLASTIC SHAPE MEMORY ALLOY IN REINFORCED CONCRETE STRUCTURES

FARAH JAAFAR & GEORGE SAAD
Department of Civil and Environmental Engineering, American University of Beirut, Lebanon

ABSTRACT

Contemporary building regulations intend to define the standards for design and construction while contemplating safety and serviceability for the occupants. Even though these codes safeguard occupants' lives under severe earthquakes, damage will occur, inducing stiff repairs and in certain cases building demolition. To address this issue, the design of buildings in seismic regions should aim to be more resilient structures that sustain little or no damage when subjected to extreme loading conditions. This study investigates the use of super-elastic shape memory alloys (SSMA) as partial replacement of steel reinforcement in reinforced concrete (RC) structures to enhance their seismic performance. SSMA is considered a particular type of smart alloys that has the ability to undergo large deformations and return to its original shape after the application of a reverse load, and hence can enhance the performance envelope of the structure. A sensitivity analysis is conducted to assess the efficiency of using SSMA at different locations in reinforced concrete frames. Fragility curves evaluating the seismic performance of an eight-story RC frame reinforced with steel and SSMA at different locations are developed. The results reveal the efficient competence of SSMA reinforced structures at different performance levels as they need greater forces to reach their plastic limit, hence increasing the overall performance of the structure.

Keywords: SSMA, performance-based design, earthquake, fragility curves.

1 INTRODUCTION

Smart materials (SM) have become topics of interest in recent research studies due to their ability to adaptively respond to external changes [1]. Depending on their type, these materials can be triggered by a change in temperature, stress or magnetic/electric field and respond by a change in their composition or properties [2]. The main advantages of SM consist of their high mechanical performance, high damping capacity, large actuation force, compactness, and lightness. Whereas SM most challenging and critical disadvantages are the high cost and environmental dependencies of these materials [3].

Shape memory alloy (SMA) is a prominent type of smart materials that have found extensive use in the engineering sector due to its two unique nonlinear phenomena, the shape memory effect (SME) and super-elasticity. The first class of SMA (SME) guarantees the recovery of large mechanical strains by heating the material above a critical temperature. On the other hand, super-elastic SMA (SSMA) has the capability to undergo large deformations and return to its original configuration upon removal of externally applied loads, without changing the ambient temperature of the system. These alloys find their applications in civil engineering due to their capability to absorb strain energy without durable damage and to withstand fatigue resistance under wide strain cycles [4]. These characteristics of SMA make it a tempting material to be used in concrete structures, especially in seismic regions. Earthquakes results in arbitrary motions, produce reversed cyclic loading on the structure, and hence can cause a compressive failure and tensile yielding of the concrete and reinforcing steel respectively [5]. Besides, large drifts may occur at the story level which leads to an increase in the structure's stiffness and a decrease in the serviceability level. Therefore, it is

WIT Transactions on The Built Environment, Vol 209, © 2022 WIT Press
www.witpress.com, ISSN 1743-3509 (on-line)
doi:10.2495/HPSU220161

a must to find an optimum design for structures to resist seismic lateral loads with minimal additional cost.

Different types of SMA have been used in concrete structures as external reinforcement (bars and rods), partial replacement of steel reinforcement (bars), for strengthening and retrofitting (wires and plates) or as fibers embedded in the cementitious composite [6]. Previous studies have experimentally outlined the relevance of SME in confining concrete elements, where an increase in the loading capacity and a decrease in the permanent deformation was noted due to the recovery stresses imposed when the SMA was heated [7]. Despite the advantages of many types of SMA, super-elastic nickel-titanium based SMA was found to be the most suitable and durable for practical use in active systems, where no external factors are needed to activate the super-elasticity effect [8]. For instance, Khaloo et al. investigated the effect of the ratio of partial reinforcement replacement by SSMA rebars on the behavior of a cantilevered reinforced concrete beam under lateral loading [9]. The study showed that SSMA material is capable of recovering its initial state, in addition to producing tensile forces which are responsible for cracks closure. Abdulridha et al. have conducted an experimental application to study the performance of a simply supported beam with SSMA bars under different loading conditions [10]. The results revealed the advantages of SSMA over regular steel in recovering large plastic deformations upon removing of loading, and hence the closure of cracks.

Many researchers have used SSMA at the plastic hinge location in different concrete elements subjected to cyclic loading to demonstrate the efficiency of this material in recovering post-yield deformations [11]. For example, Alam et al. investigated the application of SSMA in the plastic hinge area of a beam–column connection throughout a numerical analysis [12]. Their results demonstrated the superiority of SSMA–RC connection over regular steel–RC connection due the recentering capability of such material even for large deformations. Furthermore, Nahar et al. examined numerically the dynamic performance of concrete beam–columns joints reinforced with different SSMA types, at the plastic hinge location, under non-linear static pushover and reversed cycling loading. A satisfactory energy dissipation capacity and minimal residual strains were reported, which induce the least maintenance and rehabilitation cost after the post-earthquake deformation [13].

In another study, Alam et al. assessed the seismic behavior of an eight-story RC frame reinforced with SSMA along the plastic hinge length of the beams, under ten ground motion excitations, as compared to regular steel–RC frame [14]. The results showed the superiority of SSMA in reducing both inter-story and top story residual drift.

In the previously mentioned studies, the SSMA usage was confined to specific elements under specific loading conditions. Although the results demonstrated the importance of SSMA, they did not consider the probability of building damage when the location of SSMA or the intensity of loading change. Under seismic excitations, the design of buildings is probabilistic rather than deterministic, hence the importance of determining the probability of structural failure when any of the design parameters (location and length of SSMA and ground motion intensities) change. This paper addresses the missing segments in the literature by developing collapse fragility curves for RC buildings with different design parameters. This study starts by designing an eight-story steel–reinforced concrete frame (Frame 1) in a specific seismic zone. This design is replicated for two additional RC frames, where one (Frame 2) has SSMA rebars along the columns of the first floor and the second (Frame 3) is fully reinforced with SSMA along all its columns. The three frames are subjected to 21 different ground motion records and are modeled using the Open System for Earthquake Engineering Simulation (OpenSees) [15]. The collapse fragility curves are developed for the

three RC frames under increasing earthquake intensities and for different damage states. The purpose of this paper is to find the earthquake intensity margin where the performance of SSMA reinforced frames outstand that of regular steel–reinforced frame.

2 REINFORCED CONCRETE FRAME CHARACTERISTICS

The frame to be considered for analysis is designed in accordance with ACI 318-19 [16] provisions for element design, and ASCE 7-16 [17] regulations for load combination and seismic design; and it is assumed to be located in a moderate seismic zone. In compliance with the International Building Code (IBC) [18], the considered ground parameters are associated with a 475-year return period, which equates to Zone 2B [19].

2.1 Frame model

A medium rise eight-story, four bay RC frame is considered in this study, as shown in Fig. 1. The frame has a typical floor height of 4 m and span length of 5 m. The preliminary design of the frame is performed using Structural Analysis Program 2000 [20] presuming a 2D planar model and base fixation. Assuming that frame is only subjected to its own weight (D) and seismic excitation (E), the beams and columns are designed for the following load combination:

$$0.9D \pm 1E. \tag{1}$$

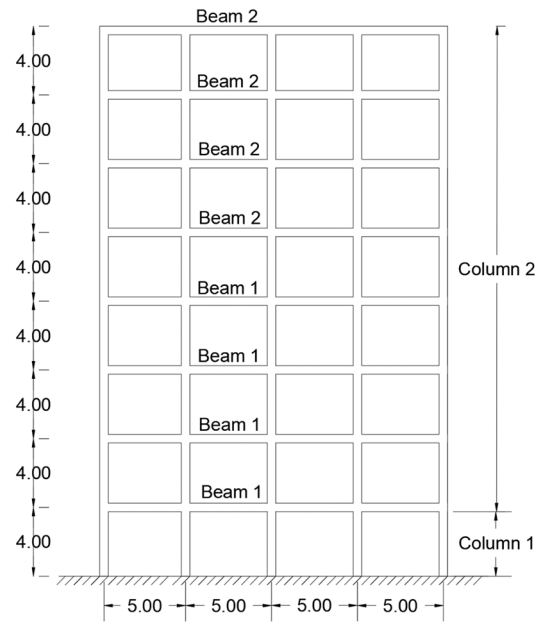

Figure 1: Eight story RC frame elevation.

The frame is designed such that it is fully reinforced with steel rebars, and its peak response is obtained from a response spectrum analysis. The response spectrum function is defined by IBC, having the following parameters:

S_s: Spectral acceleration at 0.2 s = 1.2 g

S_1: Spectral acceleration at 1 s = 0.4 g

The design response spectrum adopted is presented in Fig. 2, where T* is the first natural period of the steel reinforced concrete frame. It is evident to claim that in pursuance of a seismic analysis, the strong column–weak beam design is adopted; hence the columns are the significant elements. The beams and columns sections, in addition to the reinforcement ratio obtained from the spectral analysis are used to model the frame in Opensees. It is to be noted that only the steel reinforced frame is thoroughly designed in this study, while for the other SSMA reinforced frames, the steel rebars are simply replaced by SSMA material at certain locations.

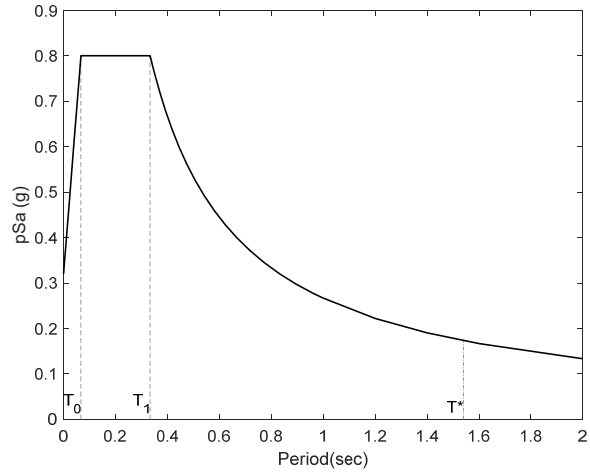

Figure 2: Design response spectrum.

2.2 Material properties

The detailed section design of Frame 1 and the material properties used in Opensees are shown in Fig. 3 and Table 1, respectively. The steel rebars are defined by Menegotto and Pinto [21] isotropic hardening material, and are assumed to be of a Grade 60, having a yielding strength of 420 MPa [22]. The SSMA bars are modeled as uniaxial self-centering material, having a flag shaped hysteretic response as shown in Fig. 4 [15]. As illustrated in Fig. 4, SSMA remains linear-elastic until the activation stress is reached, which is considered as the yielding stress in regular steel bars. Increasing the load above this limit, will cause the material to deform and plastic deformations to develop. As long as the plastic strain is less than or equal to the ultimate strain of SSMA, the material will return to its original configuration with zero residual strain upon unloading. The confined and unconfined concrete are modeled using the constitutive relationship proposed by Popovics [23] and Karsan and Jirsa [24]. The beams and columns elements are modeled using the force-beam elements (FBE), that grants the spread of plasticity along the length of the element. The convergence of FBE depends on the number of integration points along the element length, which an average of five integration points was found to be sufficient to approach the exact solution [25]. The beam and column sections are defined as fiber sections.

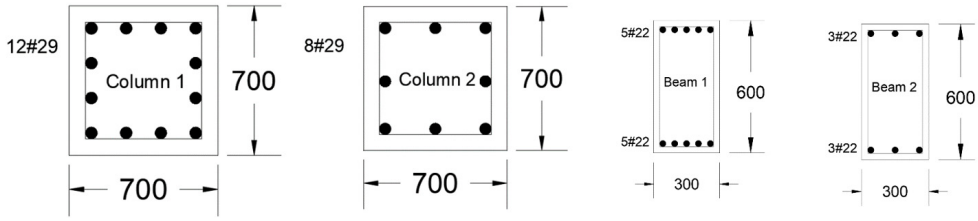

Figure 3: Columns and beams reinforcement details.

Table 1: Material properties.

Unconfined concrete	f'_c (Mpa)	30
	ε_y	0.002
	ε_u	0.004
Confined concrete	f'_{cc} (Mpa)	35.8
	ε_y	0.004
	ε_u	0.026
Steel rebars	E (Mpa)	200,000
	f_y (Mpa)	480
	εu	0.0051
SSMA rebars	K_1 (Mpa)	68,200
	σ_{act} (Mpa)	480
	K_2 (Mpa)	954.2
	ε_u	0.62

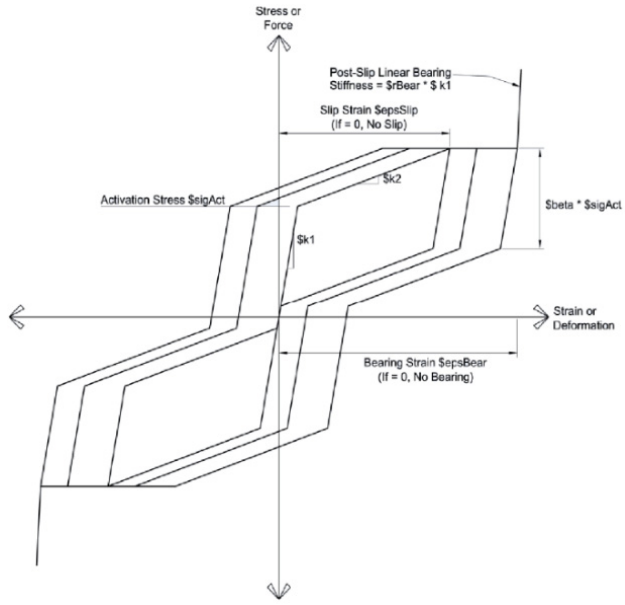

Figure 4: SSMA flag-shaped model [15].

3 NUMERICAL ANALYSES

The custom placement of SSMA is due to its high initial cost and the large deformations that can be displayed due to its low elastic stiffness. Accordingly, a dynamic uniform sine wave ground motion, with an amplitude of 4 g, is applied to the steel RC frame (Frame 1) for the sake of determining the preliminary location of SSMA. The amplitude of the ground excitation is determined such that plastic hinges start to form in the frames' vertical elements. Fig. 5 delineates the sequence of plastic hinge formation in the steel RC-frame, due to the applied ground motion. As displayed, the columns at the base were the first to deform, which is in agreement with the definition of ground shaking mechanism. Before proceeding forward, an RC frame having SSMA reinforcing bars in the columns of the first floor is subjected to the same sinusoidal excitation, to monitor the change in the plastic hinge pattern. Although the base columns are the ones to attract large forces, the plastic hinges shifted one story upward, as shown in Fig. 6. This variation of the deformation sequence is related to the different definitions of plastic hinge for both steel and SSMA reinforcement material. For instance, a plastic hinge is defined at the maximum elastic recoverable strain. In case of steel reinforcement, the latter value is nothing but the yielding strain, which is 0.0024. However, SSMA can undergo larger deformation, up to 6% strain before starting to accumulate plastic strains. Even though SSMA has a small initial stiffness as compared to steel, the large recoverable strain difference between both materials is the cause of the plastic hinge shifting.

Considering the shift of plasticity in the frame after including SSMA reinforcing bars in the first level, it may be of interest to inspect the performance of different reinforcing configurations and comparing their behaviour under seismic excitations.

Frame 1 is the originally designed steel RC frame, considered as a benchmark for comparison with SSMA–RC frames. For Frame 2, the columns reinforcing bars at the first level are replaced with SSMA bars, while all the remaining elements are reinforced with regular steel. It is veracious to say that at high earthquake intensities plastic hinges may start to form at different locations along the same member, perhaps at both ends of the base columns. To this end and to account for the all the possibilities, the assumption of having SSMA along the entire length of the column was adopted in Frame 3. It is noteworthy that these different configurations do not assume the best location of SSMA but consider the most efficient performance of the overall RC frame.

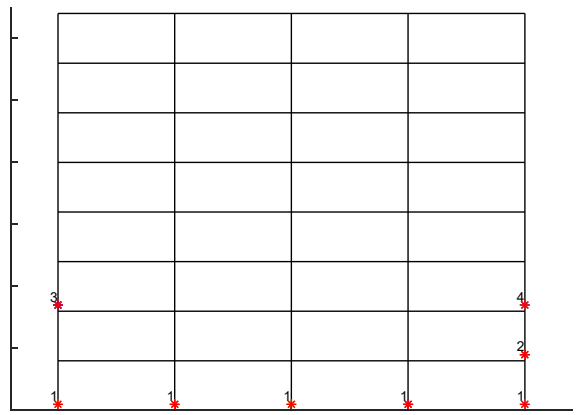

Figure 5: Plastic hinge formation of Frame 1.

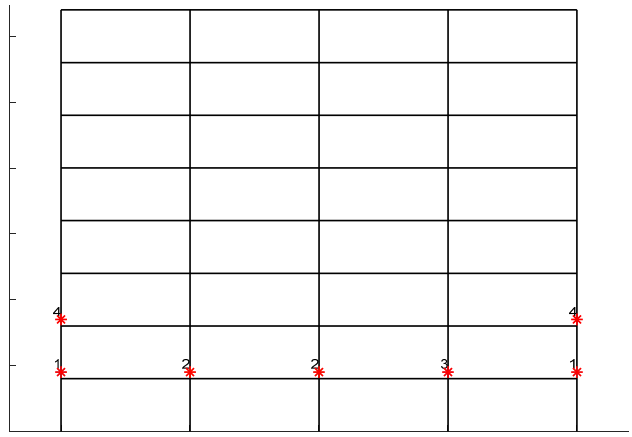

Figure 6: Plastic hinge formation of Frame 2.

It is to be noted that an eigen analysis was employed to determine the structural period for the steel RC frame (Frame 1), resulting in an average first mode period of T_1 = 1.54 s. The fundamental periods of Frames 2 and 3 are 1.56 and 1.57 respectively, which are slightly larger than that of Frame 1, as SSMA has a low stiffness compared to steel. However, for the ease of computation, a constant period is considered in this analysis. This assumption has no significant impact on the analysis since the spectral accelerations corresponding to three frames are almost identical, for a value of 0.173 g, 0.171 g and 0.1699 g respectively.

4 FRAGILITY ANALYSIS

The limited use of SSMA in the construction industry, despite its proven efficiency through numerical analysis, is associated with the high uncertainties of the global performance of the buildings reinforced with such material. According to the projects and research presented by the Pacific Earthquake Engineering Research (PEER), the seismic design of structures is probabilistic rather than deterministic. This is due to the seismic vulnerability induced by the characteristics of the structure, local site-effects, and earthquake intensity/frequency. Collapse fragility curves are widely known as the primary aspects in evaluating buildings performance. These curves aim to define a cumulative distribution function (CDF), which relates the ground motion intensity to the probability of structural failure to meet a certain response level.

In this section, the fragility functions will be developed from an incremental dynamic analysis. All three frames will be subjected to a set of 21 different ground motions scaled incrementally from a spectral acceleration ($Sa(T_1)$) 0.1g to 2g. The scale range was selected such that the frames subjected to each ground excitations fail all the performance levels stated in Table 2. The fragility function is defined by a lognormal cumulative distribution function:

$$P(C|\ IM=x) = \phi\left(\frac{\ln\left(\frac{x}{\theta}\right)}{\beta}\right), \tag{2}$$

where IM is the intensity measure adopted in the analysis, ϕ () is the standard normal cumulative function, θ is the median of the fragility function and β is the dispersion of IM. θ and β are the main parameters that define the fragility function. The procedures considered in developing the fragility curves are stated below.

Table 2: Structural performance levels.

		Structural performance levels		
Steel reinforced frame		Immediate occupancy	Life safety	Collapse prevention
	Damage	Light	Moderate	Severe
	Structure	Concrete cover is not allowed to crush in any member	Confined concrete stress $<f'_{cc}$ for all elements	Confined concrete strain in columns < cracking strain
		No yielding of steel reinforcement	Maximum steel reinforcement strain $<\varepsilon y$	Maximum steel strain< 0.0045
	Drift	Maximum drift 1%	Maximum drift 2%	Maximum drift 4%
		No significant residual drift	Maximum residual drift 1%	Maximum residual drift 4%

4.1 Define limit states

In this analysis, the probability of failure is taken for three damage states: immediate occupancy (IO), life safety (LS) and collapse prevention (CP); as per FEMA-356 [26]. All three limits account for maximum deformation, residual drift, reinforcement yielding and concrete crushing, as shown in Table 2.

It is worth mentioning that the reinforcing bars are evaluated at the stress/strain yielding limit in case of steel material and at the unrecoverable strain limit in case of SSMA.

This approach of defining the limit state is likely conservative because it assumes that when the failure limit is exceeded in one element, it triggers failure of the entire structure. In many cases, gravity loads can be redistributed to nearby elements, and the axial failure of a single column will not cause complete collapse of the frame. However, we are adopting this strategy because of physiological and psychological purposes. For example, if the maximum displacement in a story exceeds three times the allowable limit, the structure may not fail but the occupants may feel dizziness because of the large sway.

4.2 Select record set

Padgett and Desroches [27] and Asgarian et al. [28] have highlighted the effect of earthquake characteristics on the overall nonlinear performance of structural systems due to the high uncertainties provided by the random nature of these ground motions. On that account, 21 ground motions were selected with a variability in terms of magnitude, rupture fault distance, D5-95 and Arias intensity. A summary of the characteristics of the ground motions is presented in Table 3.

The considered earthquake records belong to the far field set, from Pacific Earthquake Engineering Research Center [29] strong motion database, and they are chosen such that their mean coincide with the target spectrum, as shown in Fig. 7. This set covers a wide range of earthquake properties such as frequency, ground motion intensities and duration.

4.3 Normalizing record set

The ground motions are first normalized in order to remove excessive variability between records due to the dissimilarities of the properties, in terms of magnitude, distance to source,

Table 3: Ground motions properties.

Record sequence number	Earthquake name	Magnitude	PGA (m/s^2)	Arias intensity (m/s)	5%–95% duration (s)	Normalization factor
31	Parkfield	6.19	0.272	0.4	13.1	1.2
132	Friuli Italy-02	5.91	0.212	0.4	4.6	1.28
136	Santa Barbara	5.92	0.202	0.2	7.5	1.00
162	Imperial Valley-06	6.53	0.204	0.9	14.8	0.935
204	Imperial Valley-07	5.01	0.274	0.3	6.5	0.795
208	Imperial Valley-07	5.01	0.255	0.1	7	1.002
233	Mammoth Lakes-02	5.69	0.183	0.2	7.7	1.11
236	Mammoth Lakes-03	5.91	0.233	0.4	6.3	0.907
248	Mammoth Lakes-06	5.94	0.314	0.5	6.8	1.0
249	Mammoth Lakes-06	5.94	0.377	1	5.1	0.959
391	Coalinga-03	5.38	0.199	0.2	14.8	1.288
406	Coalinga-05	5.77	0.519	0.8	8.5	0.742
408	Coalinga-05	5.77	0.193	0.3	8.5	0.997
409	Coalinga-05	5.77	0.216	0.3	8.5	0.979
410	Coalinga-05	5.77	0.309	0.6	6.9	0.852
413	Coalinga-05	5.77	0.228	0.5	6.5	1.06
456	Morgan Hill	6.19	0.213	0.2	16.6	1.131
457	Morgan Hill	6.19	0.201	0.3	20.4	1.107
502	Mt. Lewis	5.6	0.149	0.2	9.5	0.926
706	Whittier Narrows-01	5.99	0.235	0.7	9.1	1.078
714	Whittier Narrows-02	5.27	0.319	0.4	6.2	0.951

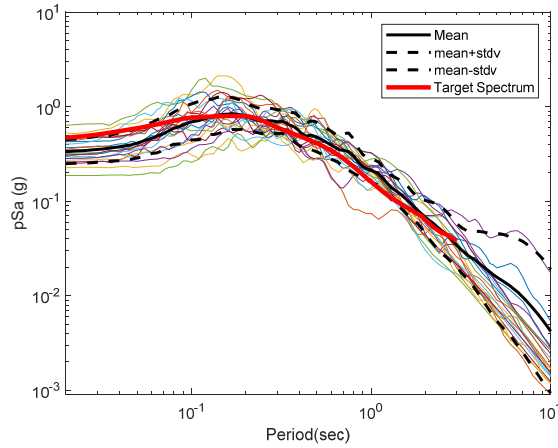

Figure 7: PEER ground motions-response spectra.

source type and site conditions, while still maintaining the record-to-record variability necessary for accurately predicting collapse fragility. The normalization is done with respect to the peak ground velocity (PGV) values. For any ground motion in the set, the normalization factor of both horizontal components is given by

$$\mathrm{CF_i} = \frac{median(PGV_{PEER,i})}{PGV_{PEER,i}}, \tag{3}$$

where $PGV_{PEER,i}$ is the geometric mean of the PGV of the two horizontal components of the *i*th ground motion in the set. Table 3 also shows the normalized factors for the ground motions set.

4.4 Define intensity measure

The intensity measure (IM) is intended to characterize the strength of the ground motion record. In the literature, the IM used are peak ground acceleration (PGA), peak ground velocity (PGV), and first-mode period damped spectral acceleration $Sa(T_1)$. However, the 5% damped first mode spectral acceleration $Sa(T_1,5\%)$ is more often adapted, because it minimizes the scatter in the results and provides a complete characterization of the response without the need for magnitude or source to site distance information [30]. Hence, $Sa(T_1)$ is considered as the intensity measure in this study.

4.5 Scaling record set

For collapse evaluation, ground motions are scaled to increasing earthquake intensities for $Sa(T_1)$ ranging between 0.1g and 2g. The scaling factor is defined by the following equation:

$$SF_{ij} = \frac{Sa_j}{CF_i * Sa_j(T)}, \tag{4}$$

where $SF_{i,j}$ is the scaling factor for the *i*th ground motion at the *j*th step in the dynamic analysis; Sa_j is the mean $Sa(T)$ of the records in the set at the *j*th step of the analysis and CF_i is the normalization factor of the *i*th record in the set. Each frame will be subjected to a set of gradually scaled earthquake records, then a nonlinear analysis will be performed to obtain the seismic response. The parameters recorded for each analysis are story drift, base reactions, confined and unconfined stresses/strains at several section in the columns and beams, and the tensile stresses in the reinforcing bars.

4.6 Developing fragility curves

Evaluating eqn (2) for a given structure requires estimating θ and β from the dynamic analysis. The lognormal distribution parameters can be determined using "Method A" approach by Porter et al. [31]

$$\theta = \frac{1}{n}\sum_{i=1}^{n} lnSa_i\,, \tag{5}$$

$$\beta = \sqrt{\frac{1}{n-1}\sum_{i=1}^{n}(lnSa_i - \theta)^2}. \tag{6}$$

where *n* is the number of ground motions considered, and Sa_i is the *Sa* value associated with onset of collapse for the *i*th ground motion.

5 RESULTS AND DISCUSSION

The fragility curves for the performance limits stated earlier are plotted in Fig. 8 with respect to $Sa(T_1)$. For each frame, three curves corresponding to each damage state are illustrated to better interpret the degree of effectiveness. All three frames have similar performance when it comes to immediate occupancy level. By observing the failure mechanism of each element in the frames throughout the dynamic analysis, the critical elements at this stage are the beams. The unconfined concrete is the first to spall in the beams of all frames; this explains the similar behavior of all frames since their horizontal elements are identical. For a life safety level, Frames 2 and 3 show a modest improvement over Frame 1 between a spectral acceleration of 0.5 g and 1.5 g. This performance level is mainly governed by confined concrete crushing in beams and reinforcement yielding in columns. The maximum drift plays a considerable role in case of SSMA–RC frames, because of the large deformation presented by SSMA bars. The outstanding performance of SSMA frames is displayed amid the collapse prevention level over a range of spectral accelerations from 0 to 3.6 g. Frame 3 surpassed Frame 2 by 5% over a small interval because of the larger drift SSMA reinforced columns present. SSMA frames are largely controlled by the maximum displacement that this smart material, by its definition, manifests.

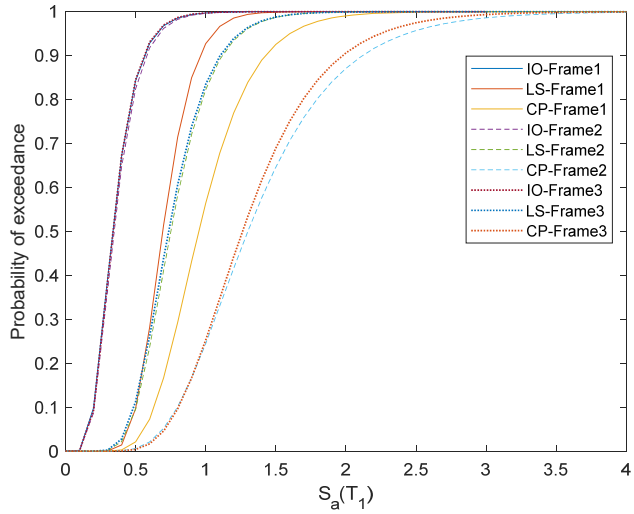

Figure 8: Fragility curves – including drifts.

Although the large deformation that an SSMA frame can undergo, as in Frame 2 for example, the vertical elements that constitute the essential components of failure are considered safe. This interpretation is better illustrated in Fig. 9, where we assumed that the maximum drift limit is not a factor that contributes to any performance level failure.

As explained earlier, the immediate occupancy is controlled by the beam behavior, so no change is expected at this level. For the second performance level, the maximum drift is one of the factors that affected the analysis in the case of SSMA–RC frames. Frames 2 and 3 surpassed Frame 1 by 40% between 0.6 g and 2 g spectral acceleration. Up to this level, replacing steel rebars by SSMA over the columns of the first floor or the entire frame is found to be invariant. This may be explained by the fact that most plastic hinges are forming at the

base level of Frame 1. By substituting the reinforcement of the first floor by SSMA rebars, the frame will need a larger force to reach its unrecoverable strain limit, hence the concrete will be subjected to minimal load until the ultimate strain is reached in SSMA.

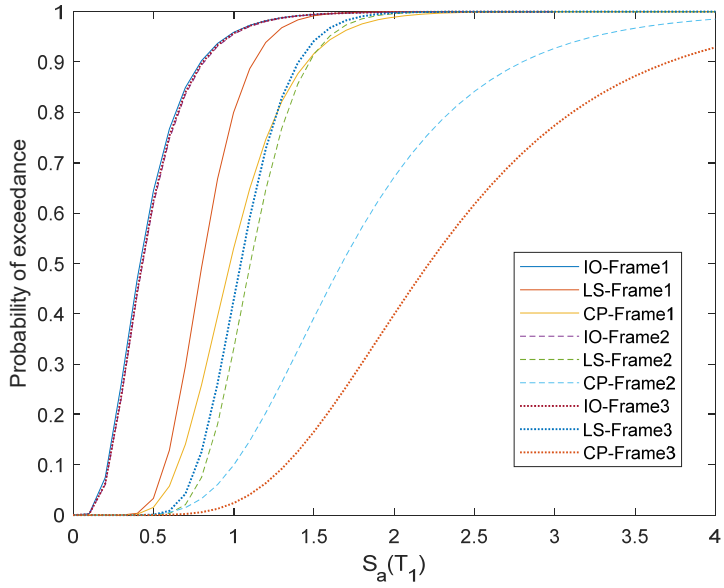

Figure 9: Fragility curves – excluding drifts.

As explained earlier, the immediate occupancy is controlled by the beam behavior, so no change is expected at this level. For the second performance level, the maximum drift is one of the factors that affected the analysis in the case of SSMA–RC frames. Frames 2 and 3 surpassed Frame 1 by 40% between 0.6 g and 2 g spectral acceleration. Up to this level, replacing steel rebars by SSMA over the columns of the first floor or the entire frame is found to be invariant. This may be explained by the fact that most plastic hinges are forming at the base level of Frame 1. By substituting the reinforcement of the first floor by SSMA rebars, the frame will need a larger force to reach its unrecoverable strain limit, hence the concrete will be subjected to minimal load until the ultimate strain is reached in SSMA.

Accordingly, confined concrete stress will be reached in Frame 1 before Frames 2 and 3. It is important to mention that the principal cause for Frame 2 to have a slightly improved performance over Frame 3 is its ability to recover plastic strains. That is to say that having a larger number of SSMA will lead to high plastic deformations, hence higher residuals. By omitting the effect of maximum displacement, it is shown that Frame 3 has the lower failure level as compared to Frames 1 and 2. Having SSMA as reinforcing bars in all the columns (Frame 3), lead to a reduction in the number plastic hinges and hence increased the overall performance. It may not be needed to have SSMA in all columns since the accumulation of plastic hinges will be essentially in the bottom floors. On that account, further SSMA configurations need to be considered to achieve the best performance level with the minimum material cost.

6 CONCLUSIONS

The aim of this study is to demonstrate the advantages of using SSMA in RC frames for different performance levels, as compared to regular steel RC frame. Since the base columns are more susceptible to damage during earthquake, the first SSMA–RC frame was reinforced by SSMA bars at the base columns. To account for additional plastic hinge formation during severe earthquakes, another RC frame reinforced with SSMA along all its columns, is used. The seismic performance of the three frames was compared using the fragility analysis. The frames were subjected to 21 incrementally scaled ground motions, where the stresses/strains in columns and beams were recorded, in addition to the drift and residual displacement. The results of the analysis are as follow:

- SSMA requires larger tensile forces to reach plastic strains due to the lower stiffness of this material; hence higher ground motion intensities are needed to reach failure.
- For an immediate occupancy performance level, steel frame showed similar behavior to both SSMA frames since the beams were the key elements at this stage. An addition frame having its beams reinforced with SSMA bars could be useful for further investigations.
- The number of SSMA bars is crucial, as the larger the steel to SSMA ratio is, the higher the deformations are. Thereby, the recovery capacity will be reduced, and the repair cost will increase.
- Since SSMA is the slowest to reach unrecoverable strain limit, it will attract both tensile and compressive stresses generated by the ground excitation, therefore the concrete part will be subjected to negligeable stresses, and the concrete failure will be delayed.

The maximum displacement of an RC frame can be dismissed from the failure criteria of a specific performance level since it may be a misleading indicator of failure; specially in case of SSMA–RC frames. The fragility analysis highlighted the efficiency of using SSMA in RC frames for both life safety and collapse prevention performance levels. The number of SSMA bars to be used and their locations are concerns to be addressed in further studies, for economical and structural purposes.

REFERENCES

[1] Takagi, T., A concept of intelligent materials. *Journal of Intelligent Material Systems and Structures,* **1**(2), pp. 149–156, 1990. DOI: 10.1177/1045389X9000100201.

[2] Reece, P., *Smart Materials and Structures: New Research*, Nova Science Publishers: New York, 2007.

[3] Mehrpouya, M. & Bidsorkhi, H., MEMS applications of NiTi based shape memory alloys: A review. *Micro and Nanosystems,* **8**(2), pp. 79–91, 2017. DOI: 10.2174/1876402908666161102151453.

[4] Mir, B.A., Smart materials and their applications in civil engineering: An overview. *International Journal of Civil Engineering and Construction Science*, pp. 11–20, 2017.

[5] Murty, C.V.R., https://www.iitk.ac.in/nicee/EQTips/EQTip17.pdf.

[6] Molod, M.A., Spyridia, P. & Barthold, F-J., Applications of shape memory alloys in structural engineering with a focus on concrete construction: A comprehensive review. *Construction and Building Materials*, **337**, 127565, 2022. DOI: 10.1016/j.conbuildmat.2022.127565.

[7] Hong, C., Qian, H. & Song, G., Uniaxial compressive behavior of concrete columns confined with superelastic shape memory alloy wires. *Materials*, **13**(5), p. 1227, 2020. DOI: 10.3390/ma13051227.

[8] Hamid, N.A., Ibrahim, A. & Adnan, A., Behaviour of smart reinforced concrete beam with super elastic shape memory alloy subjected to monotonic loading. *AIP Conference Proceedings*, **1958**, 020034, 2018. DOI: 10.1063/1.5034565.
[9] Khaloo, A.R., Eshghi, I. & Aghl, P.P., Study of behavior of reinforced concrete beams with smart rebars using finite element modeling. *International Journal of Civil Engineering*, **8**(3), 2010.
[10] Abdulridha, A., Palermo, D., Foo, S. & Vecchio, F.J., Behavior and modeling of superelastic shape memory alloy reinforced concrete beams. *Engineering Structures,* pp. 893–904, 2013. DOI: 10.1016/j.engstruct.2012.12.041.
[11] Saiidi, M.S. & Wang, H., Exploratory study of seismic response of concrete columns with shape memory alloys reinforcement. *ACI Structural Journal*, **103**(3), pp. 436–443, 2006. DOI: 10.14359/15322.
[12] Alam, S., Youssef, A. & Nehdi, M., Seismic behaviour of concrete beam-column joints reinforced with superelastic shape memory alloys. *9th Canadian Conference on Earthquake Engineering,* Canada, 2007. DOI: 10.13140/2.1.4516.0966.
[13] Nahar, M., Muntasir Billah, A.H.M., Kamal, H.R. & Islam, K., Numerical seismic performance evaluation of concrete beam-column joint reinforced with different super elastic shape memory alloy rebars. *Engineering Structures*, **194**, pp. 161–172, 2019. DOI: 10.1016/j.engstruct.2019.05.054.
[14] Alam, S., Nedi, M. & Youssef, M., Seismic performance of concrete frame structures reinforced with superelastic shape memory alloys. *Smart Structures and Systems,* pp. 565–585, 2009. DOI: 10.12989/sss.2009.5.5.565.
[15] McKenna, F., Fenves L. & Scott H., Open System for Earthquake Engineering Simulation (OpenSees). *Pacific Earthquake Engineering Research Center*, 2000.
[16] ACI 318-19, Building code requirements for structural concrete. American Concrete Institute: Farmington Hills, MI, USA, 2020.
[17] ASCE/SEI 7-16*,* Minimum design loads and associated criteria for buildings and other structures, American Society of Civil Engineers, 2017.
[18] IBC*,* International building code, Virginia, 2020.
[19] Aarango, M. & Lubkowski Z., Seismic hazard assessment and design requirements for Beirut, Lebanon. *15th World Conference in Earthquake Engineering,* Lisbon, 2012.
[20] SAP2000, Integrated structural analysis and design software. *Computer and Structures*, 1997.
[21] Menegotto, M. & Pinto, P.E., Method of analysis of cyclically RC plane frames including changes in geometry and non-elastic behavior of elements under normal force and bending. *Materials Science*, pp. 15–22, 1973. DOI: 10.5169/seals-13741.
[22] Anggraini, R., Tavio, I., Raka, G.P. & Agustiar, Stress-strain relationship of high-strength steel (HSS) reinforcing bars. *AIP Conference Proceedings*, **1964**, 020025, 2018. DOI: 10.1063/1.5034565.
[23] Popovics, S., A numerical approach to the complete stress strain curve for concrete. *Cement and Concrete Research,* pp. 583–599, 1973. DOI: 10.1016/0008-8846(73)90096-3.
[24] Karsan, D. & Jirsa O., Behavior of concrete under compressive loading. *Journal of Structural Division ASCE*, 1969. DOI: 10.1061/JSDEAG.0002424.
[25] Scott, M.H., A tale of two element formulations. Portwood Digital, 2020. https://portwooddigital.com/2020/02/23/a-tale-of-two-element-formulations/.
[26] FEMA-356*, Handbook for the Seismic Evaluation of Buildings: A Prestandard and Commentary for Seismic Rehabilitation of Buildings*, The American Society of Civil Engineers for the Federal Emergency Management Agency: Washington, DC, 2000.

[27] Padgett, J. & Desroches, R., Sensitivity of seismic response and fragility to parameter uncertainty. *Journal of Structural Engineering*, **133**(12), 2007. DOI: 10.1061/(asce)0733-9445(2007)133:12(1710).
[28] Asgarian, B., Salehi, E. & Shokrgozar, H., Probabilistic seismic evaluation of buckling restrained braced frames using DCFD and PSDA methods. *Earthquakes and Structures*, **10**(1), pp. 1–19, 2016. DOI: 10.12989/eas.2016.10.1.105.
[29] PEER Ground Motion Database, University of California, Berkeley, 2014.
[30] Carballo, J.E. & Cornell, C.A., Probabilistic seismic demand analysis: Spectrum matching and design. Reliability of marine structures program, Report No. RMS-41, Stanford University, USA, 2000.
[31] Porter, K., Kennedy, R. & Bachman R., Creating fragility functions for performance-based earthquake engineering. *Earhquake Spectra*, pp. 471–489, 2007. DOI: 10.1193/1.2720892.